

industrial areas, the acknowledged targets of these nations, they would start fires, producing massive amounts of smoke. That smoke would block out sunlight, making it cold and dark at the surface for many years, as well as destroy ozone, enhancing ultraviolet radiation reaching the surface (e.g., Mills et al., 2014). The size of these impacts would depend on the number and yield of the nuclear weapons used, as well as the specific targets.

In the past decade, climate model simulations, which used a coupled atmosphere-ocean general circulation model run continuously for multiple 10-year simulations and with a model top at the mesopause, have supported the conclusion that full-scale global nuclear war can still produce a nuclear winter (Robock, Oman, & Stenchikov, 2007). In addition, several groups found that a nuclear war between new nuclear states such as India and Pakistan, using much less than 1% of the current global nuclear arsenal, could produce climate change unprecedented in recorded human history (Mills et al., 2014; Pausata et al., 2016; Robock, Oman, Stenchikov, et al., 2007; Stenke et al., 2013; Toon, Robock, et al., 2007; Toon, Turco, et al., 2007), global-scale ozone depletion (Mills et al., 2008, 2014), and widespread famine (Özdogan et al., 2013; Xia et al., 2015; Xia & Robock, 2013).

All these results are model simulations. Is there any way to test the climatic response to stratospheric soot from observations? Unfortunately, history presents us with examples of cities that have burned in the past. Accidental fires burned numerous cities, including London in 1666, Chicago in 1871, and San Francisco in 1906. About the San Francisco fire, which was started by an earthquake, London (1906) wrote, "Not in history has a modern imperial city been so completely destroyed. San Francisco is gone." Yet, during World War II, cities were burned intentionally (Caidin, 1960; The U.S. Strategic Bombing Survey, 1946).

"In the attacks on German cities incendiary bombs, ton for ton, were found to have been between four and five times as destructive as high explosive. ... in the more serious fire raids, any fire-fighting equipment was found to have been of little avail. Fire storms occurred, the widespread fires generating a violent hurricane-like draft, which fed other fires and made all attempts at control hopeless. ... 485,000 residential buildings were totally destroyed by air attack and 415,000 were heavily damaged, making a total of 20 percent of all dwelling units in Germany. In some 50 cities that were primary targets of air attack, the proportion of destroyed or heavily damaged dwelling units is about 40 percent. The result of all these attacks was to render homeless some 7,500,000 German civilians." (The U.S. Strategic Bombing Survey, 1945).

And certainly these fires produced smoke plumes. In Japan, "Greatest source of alarm to our flyers were the terrific thermals, or hot-air currents, that rose from the blazing targets and sent our aircraft into a black hell of smoke" (Caidin, 1960, p. 154). "We headed into a great mushroom of boiling, oily smoke, and in a few seconds were tossed 5,000 feet [1,500 m] into the air" (Caidin, 1960, pp. 154–155). As London (1906) described for the San Francisco fire,

"Within an hour after the earthquake shock the smoke of San Francisco's burning was a lurid tower visible a hundred miles [160 km] away. And for three days and nights this lurid tower swayed in the sky, reddening the sun, darkening the day, and filling the land with smoke. ... I watched the vast conflagration from out on the bay. It was dead calm. Not a flicker of wind stirred. Yet from every side wind was pouring in upon the doomed city. East, west, north, and south, strong winds were blowing upon the doomed city. The heated air rising made an enormous suck. Thus did the fire of itself build its own colossal chimney through the atmosphere. Day and night this dead calm continued, and yet, near the flames, the wind was often half a gale, so mighty was the suck."

In the next section we estimate the smoke from these World War II city fires, the effects on solar irradiance and radiative forcing, and the potential climate impact. Then we compare those estimates to global surface air temperature observations and to climate model simulations.

2. Uncertainties

All these records have large uncertainties. We have good data on the cities that burned, but not on their fuel loading, smoke emissions, or plume heights. Available solar irradiance observations are from two sites only

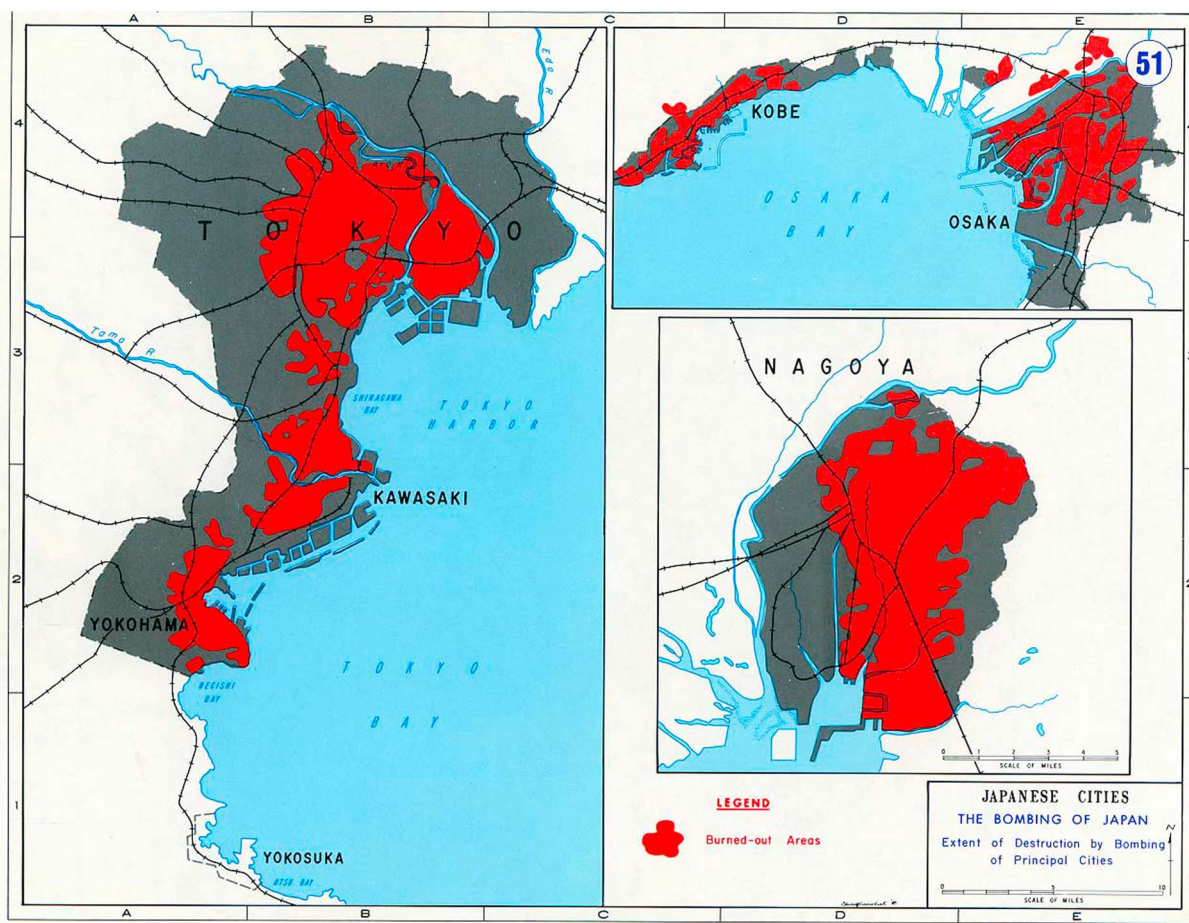


Figure 1. Extent of destruction by U.S. bombing of major Japanese cities in 1945 (from United States Military Academy History Department Atlas, <http://www.usma.edu/history/SiteAssets/SitePages/World%20War%20II%20Pacific/ww%20asia%20map%2051.jpg>).

and, although taken on mountaintops, still are affected by the troposphere, thin clouds, and potential errors in the instruments. Sea surface temperature observations during the period of World War II were affected by changing observing techniques and locations, necessitating the use of only surface air temperatures over land. The 1940–1942 El Niño did not produce global warming because of a circulation response that produced cooling over land (Brönnimann et al., 2004), while the La Niñas of 1950 and 1956 did produce global land cooling.

3. Smoke Emissions

Toon, Turco, et al. (2007) provided a method for estimating the smoke emissions from burning cities, taking account of the amount of fuel per capita and integrating over population densities in different cities, and assuming the area burned in each case would be the area of Hiroshima that burned (13 km^2) as a result of the atomic bombing on 6 August 1945. Here, because for Japan we know the total area burned, we simplify the approach as

$$M = A F E R L \quad (1)$$

where M is the total mass of soot injected into the lower stratosphere (kg), A is the total area burned (m^2), F is the total fuel per unit area (kg/m^2), E is the percent of fuel that is emitted as soot into the upper troposphere (%), R is the fraction that is not rained out (%), and L is the fraction lofted from the upper troposphere into the lower stratosphere, either injected directly or by subsequent solar heating (%). Caidin (1960) described how the B-29 Superfortress bomber was created in secret as a high-altitude (over 30,000 ft. [9,100 m]), long-range



Figure 2. Part of Shizuoka after it was firebombed on 19 June 1945, (<http://www.japanairraids.org/wp-content/uploads/2010/10/A3823.jpg>).

bomber (over 5,000 km) for use by the United States in World War II. Caidin (1960) reported that in Japan, starting with the firebombing of Kobe on the night of 3 February 1945 through the atomic bombing of Nagasaki on 9 August 1945, “the Superfortresses had gutted a total of 178 square miles [461 km²] in 69 cities,” which included the destruction of over 50% of Tokyo, Yokohama, and Kobe (Figure 1). Figure 2 shows part of Shizuoka, as an example, where 66% was destroyed by incendiary bombs. Toon, Turco, et al. (2007) reported a range of values for F and E depending on the city and year but assumed a value of 1.6 kg/m² for F for Hiroshima and 1.6% for E . They also estimate R to be 80%.

As Toon, Turco, et al. (2007) explained, for fires with a diameter exceeding the atmospheric scale height (about 8 km), pyro-convection would directly inject soot into the lower stratosphere. And while we know of no observations of this from the World War II fires, Fromm et al. (2010, 2008) have described the 2001 Chisholm forest fire in Alberta, Canada, which was observed to directly inject about the same amount of smoke into the stratosphere as expected from one Hiroshima-sized firestorm. Fromm et al. (2010) described numerous other such natural fires. Although they were scattered in time and space and did not have as much fuel, they still produced small stratospheric injections. However, even if the initial smoke injection from city fires only had enough lofting to get the smoke into the upper troposphere, subsequent solar heating would loft it into the lower stratosphere in the summer in midlatitudes, as calculated by Toon, Turco, et al. (2007) and as observed after the August 2017 pyrocumulonimbus injection from British Columbia forest fires (e.g., Ansmann et al., 2018; Peterson et al., 2018). Because the city fires were at nighttime and did not always persist until daylight, and because some of the city fires were in the spring, with less intense sunlight, we estimate that L is about 0.5, so based on the values above, M for Japan for the summer of 1945 was about 0.5 Tg of soot. However, this estimate is extremely uncertain.

For Europe, although Hamburg (July 1943), Darmstadt (September 1944), Dresden (February 1945; Vonnegut, 1969), and Dortmund (March 1945) were destroyed by firestorms, much of the destruction in Europe was from high-explosive bombs and not fires. The total area in Germany bombed in the entire war was an estimated 205 km² (Murray & Millett, 2000). The smoke emissions were also spread out over 6 years, starting with the Blitz raids on England in 1940 through the final bombings of Germany ending in Lübeck (April 1945). Fifty-eight percent of the total bombing tonnage on Germany took place in 1944, 23% in 1945, and only



Figure 3. The Mt. Montezuma, Chile (Smithsonian Institution Archive. Image # 2003-19480) solar irradiance observatory.

19% in the preceding years http://humanities.exeter.ac.uk/media/universityofexeter/collegeofhumanities/history/researchcentres/centreforthestudyofwarstateandsociety/bombing/THE_BOMBING_OF_GERMANY.pdf. With the same assumptions as for Japan, the smoke emissions from Germany from equation (1) would amount to about 0.1 Tg of soot emitted to the stratosphere in 1944 and an additional 0.05 Tg in 1945.

4. Impacts on Solar Irradiance

As discussed by Hoyt (1979), the Smithsonian Astrophysical Observatory (then abbreviated APO) Solar Constant Program (Aldrich & Hoover, 1954) maintained two long-term observatories of the solar constant (now called *solar irradiance*) at Mt. Montezuma, Chile ($22^{\circ}40'S$, $68^{\circ}56'W$; Figure 3) and Table Mountain, California, USA ($34^{\circ}22'N$, $117^{\circ}41'W$; Figure 4). While they adjusted their measurements for Rayleigh scattering, clouds, and water vapor, and tried to remove polluted days,

"it appears that the influence of aerosol scattering was not entirely removed from the derivation of the solar constant values. Throughout the APO program the solar constant reduction scheme never handled the problem of aerosols or volcanic dust properly." (Hoyt, 1979, p. 440).

Hence, we might expect this record to include changes of stratospheric aerosols. Indeed Aldrich and Hoover (1954) and Hoyt (1979) commented on the reductions in solar irradiance in 1932 because of volcanic eruptions in Chile.

Figure 5 shows the solar irradiance observations for 1923–1953. The effects of the 10–11 April 1932 Quizapu volcanic eruption in Chile are clear, as are the effects of "solar dimming" from tropospheric pollution beginning around 1950 (Wild, 2009).

The lowest values during World War II were in 1944 and 1945, with solar irradiance about 3 W/m^2 below the background values, defined as the average for 1940–1943 ($1,358.4\text{ W/m}^2$), indicated as a purple line in Figure 5. Accounting for a planetary albedo of about 0.3 and the spherical shape of Earth, this would amount to a radiative forcing of about -0.5 W/m^2 .

Figure 5 also shows observations of sunspot numbers for the same period. Aldrich and Hoover (1954) suggested that part of the decadal variations of solar irradiance were due to changes in solar emission correlated with the sunspot number. However, Kopp and Lean (2011), using modern satellite observations of total solar irradiance, found that solar irradiance varies by about 1.6 W/m^2 between solar maximum and solar minimum, independent of the sunspot value at solar maximum. Since the observations of solar irradiance in Figure 5



Figure 4. Table Mountain, California (Smithsonian Institution Archive. Image # MAH-21248B) solar irradiance observatory.

vary by 10 W/m^2 between solar maximum and solar minimum, the effect of sunspots cannot explain more than a small amount of that variation. In addition, the solar irradiance and sunspot numbers are not correlated for the first part of the record.

An alternative explanation for the reduction of insolation in 1944 and 1945 is tropospheric pollution from industrial activity. However, U.S. industrial production peaked in February 1944, stayed relatively flat until February 1945, and then plummeted during 1945 to a low in October 1945 (Board of Governors of the Federal Reserve System (U.S.), 2017). The period February–October, 1945, was labeled as a recession. By the end of 1945, U.S. industrial production had fallen to 2/3 of its value in 1944. Similarly, industrial production in Germany (Grayling, 2006) and Japan (Caidin, 1960) was drastically diminished by bombing by 1945.

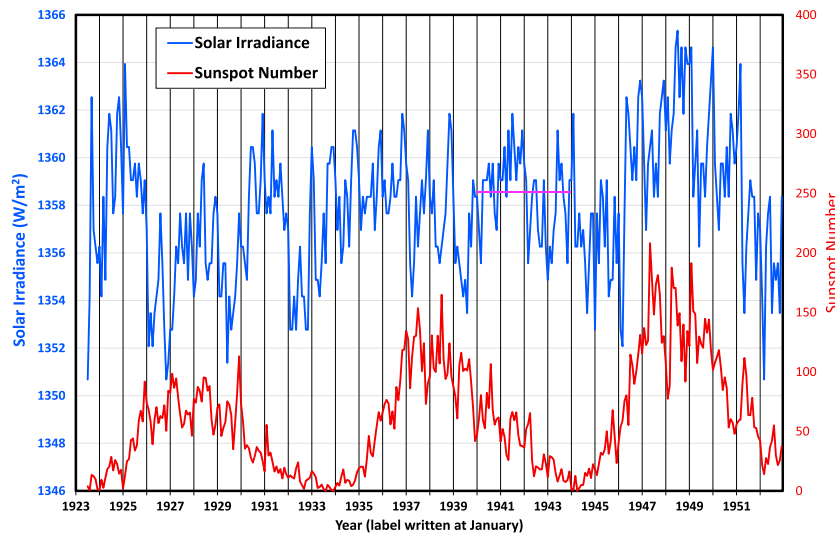


Figure 5. Monthly average solar irradiance and sunspot number observations. Data from Table 17 in Aldrich and Hoover (1954). The effects of the 10–11 April 1932 Quizapu volcanic eruption in Chile are clear, as are the effects of “solar dimming” from tropospheric pollution beginning around 1950. The purple line is the background solar irradiance during 1940–1943 (1358.4 W/m^2).

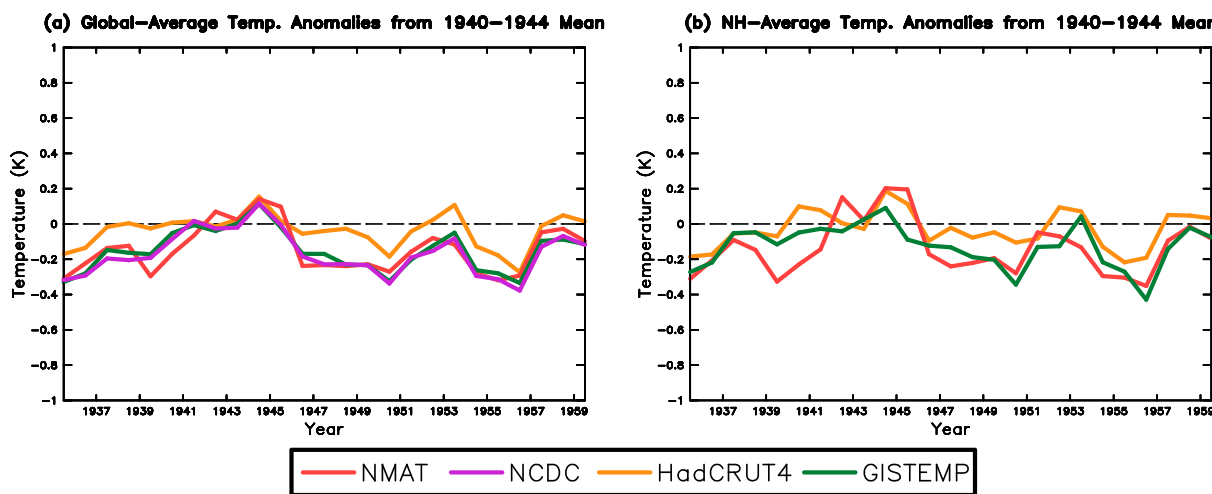


Figure 6. (a) Global and (b) Northern Hemisphere (NH) annual average temperature anomaly (K) with respect to 1940–1944 mean. Shown are combined ocean and land surface air temperature from National Climatic Data Center (NCDC) Merged Land-Ocean Surface Temperature Analysis (Smith et al., 2008), HadCRUT4 Reanalysis (Morice et al., 2012), and GISTEMP (GISTEMP team, 2016; Hansen et al., 2010), and ocean-only temperatures from the Hadley Centre Nighttime Marine Air Temperature (NMAT; Kent et al., 2013). GISTEMP = Goddard Institute for Space Studies Surface Temperature Analysis.

Tropospheric aerosols have an e-folding lifetime of only about 1 week. So their effect would have been much larger in 1944 than 1945, yet we found a larger insolation reduction in 1945 (average solar insolation of 1356.4 W/m^2) as compared to 1944 (average solar insolation of 1357.0 W/m^2). Most likely, the reduction in 1944 was partially from tropospheric aerosols, but in 1945 may have been from stratospheric soot.

5. Temperature Observations

Sea surface temperature observations during the period of World War II and afterwards had several problems. Observers, to avoid being attacked by using lights on deck at night after bringing up a bucket of water to measure, would bring the buckets inside the cabin, which would artificially warm the water. In addition, there was a switch from bucket to intake temperatures soon after the war and there were different shipping patterns during the war, all of which contributed to a large drop from 1945 to 1946 of about 0.3 K (Figure 6), which does not represent the actual temperature variation (Thompson et al., 2008).

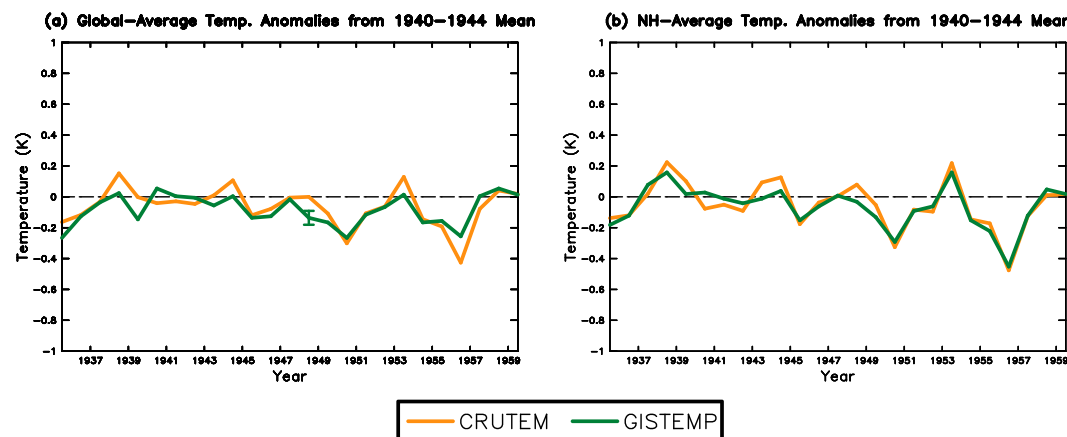


Figure 7. (a) Global and (b) Northern Hemisphere (NH) annual average land surface air temperature anomaly (K) with respect to 1940–1944 mean. Data are from CRUTEM (Jones et al., 2012; Osborn & Jones, 2014) and GISTEMP (GISTEMP team, 2016; Hansen et al., 2010). The green whisker (plotted at 1948 in (a)) is the uncertainty of the GISTEMP observations (95% confidence limit) accounting only for incomplete spatial sampling (Hansen et al., 2010). CRUTEM = Climatic Research Unit TEMperature data set. GISTEMP = Goddard Institute for Space Studies Surface Temperature Analysis.

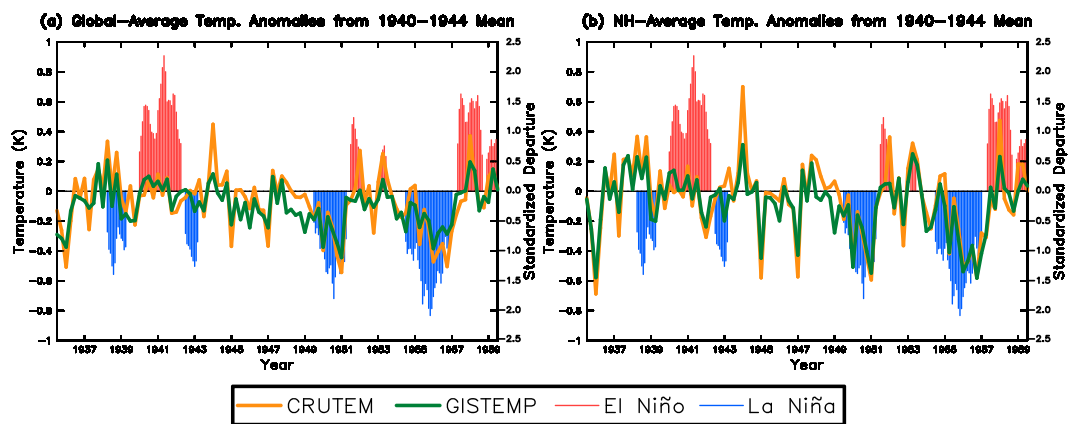


Figure 8. (a) Global and (b) Northern Hemisphere seasonal average land surface air temperature anomaly (K) with respect to 1940–1944 mean. Data are from CRUTEM (Jones et al., 2012; Osborn & Jones, 2014) and GISTEMP (GISTEMP team, 2016; Hansen et al., 2010). Vertical red and blue lines indicate El Niño and La Niña events, reconstructed using the Multivariate ENSO Index (units on right axes, Wolter & Timlin, 2011). ENSO = El Niño Southern Oscillation; CRUTEM = Climatic Research Unit TEMperature data set; GISTEMP = Goddard Institute for Space Studies Surface Temperature Analysis. Abscissa tick marks are for January of each year.

Because of these issues, we decided to use only land surface air temperatures in our analysis. Figure 7 shows annual-average global mean or Northern Hemisphere (NH) surface air temperature only over land from the two standard analyses from the Goddard Institute for Space Studies (GISTEMP team, 2016; Hansen et al., 2010) and the Climatic Research Unit (Jones et al., 2012; Osborn & Jones, 2014), and both show a drop in 1945 of about 0.1 K in global average temperature, and 0.2 K in NH average temperature, with about half that drop in 1946.

However, when we break up the record into seasonal rather than annual averages, it is seen in Figure 8 that the cooling in 1945 occurred at the beginning of the year, before any smoke would have been injected into the stratosphere. While this cooling in early 1945 may have been due to natural variability, the clear annual signal for 1945 cannot have been caused solely by stratospheric smoke. There were no large volcanic eruptions and no El Niño or La Niña in 1945 or 1946. The other large temperature drops in the record are centered

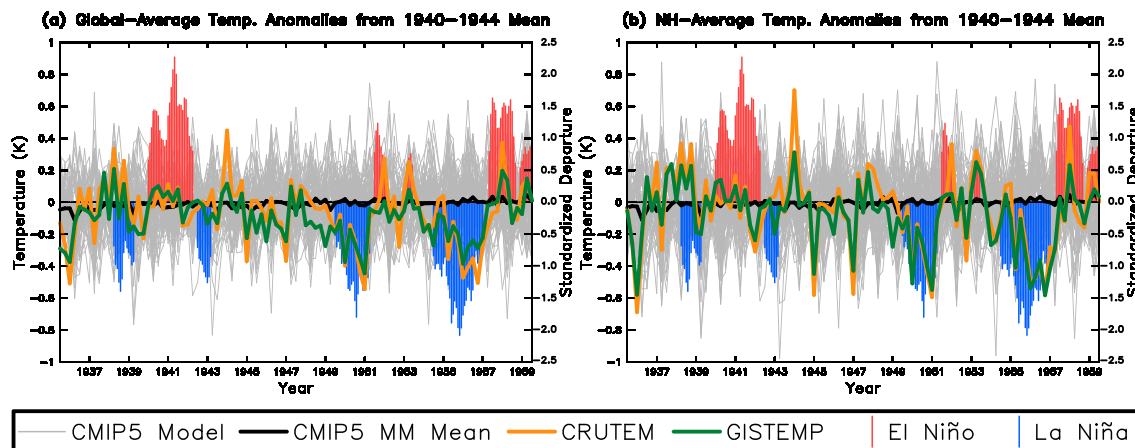


Figure 9. (a) Global and (b) Northern Hemisphere seasonal average land surface air temperature anomalies, with respect to the average for 1940–1944, from the CMIP5 historical simulations (Table 1), and observations from CRUTEM (Jones et al., 2012; Osborn & Jones, 2014) and GISTEMP (GISTEMP team, 2016; Hansen et al., 2010). The thin gray lines are the first three ensemble members for each separate climate model (Table 1), and the thick black line is the multimodel mean. Vertical red and blue lines indicate El Niño and La Niña events, reconstructed using the Multivariate ENSO Index (Wolter & Timlin, 2011). CMIP5 = Coupled Model Intercomparison Project 5; GISTEMP = Goddard Institute for Space Studies Surface Temperature Analysis; ENSO = El Niño Southern Oscillation. Abscissa tick marks are for January of each year.

- Turco, R. P., Toon, O. B., Ackerman, T. P., Pollack, J. B., & Sagan, C. (1983). Nuclear winter: Global consequences of multiple nuclear explosions. *Science*, 222(4630), 1283–1292. <https://doi.org/10.1126/science.222.4630.1283>
- Voldoire, A., Sanchez-Gomez, E., Salas y Mélia, D., Decharme, B., Cassou, C., Sénési, S., et al. (2012). The CNRM-CM5.1 global climate model: Description and basic evaluation. *Climate Dynamics*, 40(9–10), 2091–2121. <https://doi.org/10.1007/s00382-011-1259-y>
- Vonnegut, K. (1969). *Slaughterhouse-Five, or The Children's Crusade: A duty-dance with death* (205 pp.). New York: Delacorte Press.
- Watanabe, S., Hajima, T., Sudo, K., Nagashima, T., Takemura, T., Okajima, H., et al. (2011). MIROC-ESM 2010: Model description and basic results of CMIP5-20c3m experiments. *Geoscientific Model Development*, 4(4), 845–872. <https://doi.org/10.5194/gmd-4-845-2011>
- Watanabe, M., Suzuki, T., Oishi, R., Komuro, Y., Watanabe, S., Emori, S., et al. (2010). Improved climate simulation by MIROC5: Mean states, variability, and climate sensitivity. *Journal of Climate*, 23(23), 6312–6335. <https://doi.org/10.1175/2010JCLI3679.1>
- Wild, M. (2009). Global dimming and brightening: A review. *Journal of Geophysical Research*, 114, D00D16. <https://doi.org/10.1029/2008JD011470>
- Wolter, K., & Timlin, M. S. (2011). El Niño/Southern Oscillation behaviour since 1871 as diagnosed in an extended multivariate ENSO index (MEI.ext). *International Journal of Climatology*, 31(7), 1074–1087. <https://doi.org/10.1002/joc.2336>
- Wu, T., Li, W., Ji, J., Xin, X., Li, L., Wang, Z., et al. (2013). Global carbon budgets simulated by the Beijing Climate Center Climate System Model for the last century. *Journal of Geophysical Research: Atmospheres*, 118, 4326–4347. <https://doi.org/10.1002/jgrd.50320>
- Xia, L., & Robock, A. (2013). Impacts of a nuclear war in South Asia on rice production in mainland China. *Climatic Change*, 116(2), 357–372. <https://doi.org/10.1007/s10584-012-0475-8>
- Xia, L., Robock, A., Mills, M., Stenke, A., & Helfand, I. (2015). Decadal reduction of Chinese agriculture after a regional nuclear war. *Earth's Future*, 3(2), 37–48. <https://doi.org/10.1002/2014EF000283>
- Yukimoto, S., Adachi, Y., Hosaka, M., Sakami, T., Yoshimura, H., Hirabara, M., et al. (2012). A new global climate model of the Meteorological Research Institute: MRI-CGCM3 model description and basic performance. *Journal of the Meteorological Society of Japan*, 90A, 23–64. <https://doi.org/10.2151/jmsj.2012-A02>